JACS
JOURNAL OF THE AMERICAN CHEMICAL SOCIETY

COMMUNICATION

pubs.acs.org/JACS

High Activity Carbide Supported Catalysts for Water Gas Shift

Neil M. Schweitzer,[†,‡] Joshua A. Schaidle,[†,‡] Obiefune K. Ezekoye,[§] Xiaoqing Pan,[§] Suljo Linic,[‡] and Levi T. Thompson*[,†,‡]

[†]Hydrogen Energy Technology Laboratory, [‡] Department of Chemical Engineering, and [§]Department of Materials Science and Engineering, University of Michigan, Ann Arbor, Michigan 48109, United States

Supporting Information

ABSTRACT: Nanostructured carbides are refractory materials with high surface areas that could be used as alternatives to the oxide materials that are widely used as support materials for heterogeneous catalysts. Carbides are also catalytically active for a variety of reactions, offering additional opportunities to tune the overall performance of the catalyst. In this paper we describe the synthesis of molybdenum carbide supported platinum (Pt/Mo_2C) catalysts and their rates for the water gas shift reaction. The synthesis method allowed interaction of the metal precursor with the native, unpassivated support. The resulting materials possessed very high WGS rates and atypical Pt particle morphologies. Under differential conditions, rates for these catalysts were higher than those for the most active oxide-supported Pt catalysts and a commercial Cu−Zn−Al catalyst. Experimental and computational results suggested that active sites on the Pt/Mo_2C catalysts were located on the perimeter of the Pt particles and that strong interactions between Pt and the Mo_2C surface gave rise to raft-like particles.

Early transition metal carbides (e.g., molybdenum carbide, Mo_2C) have been demonstrated to be catalytically active for reactions ranging from hydrogenolysis[1] to isomerization.[2] Because of their high surface areas (sometimes exceeding 200 m^2/g), thermal stabilities, and electronic conductivities,[3] carbides are also attractive for use as catalyst and electrocatalyst supports. However, only a few investigations have been reported regarding their use for this purpose. Lewandowski et al., for example, dispersed Pt on Mo_2C and found the resulting material to be highly active for hydrodenitrogenation and hydrodesulfurization reactions.[4] Griboval-Constant et al. reported that supporting Co or Ru onto Mo_2C produced catalysts with high Fischer−Tropsch synthesis activities and favorable product selectivities.[5] In these studies, the metals were deposited onto passivated Mo_2C powders (carbides are typically passivated prior to exposure to air due to their pyrophoricity). Therefore, the metal precursors interacted with an oxidized surface rather than the native carbide surface.

A key objective of our research has been to synthesize and characterize materials where the metals interact directly with the native surfaces of high surface area carbides. To accomplish this objective, we developed a technique to deposit metals directly onto carbide surfaces using an aqueous wet impregnation method. A key to this method is avoiding exposure of the carbide surface to O_2, by, among other things, deaerating the aqueous metal precursor solution. Carbides are oxidized spontaneously by O_2; however, oxidation by liquid water is thermodynamically unfavorable (see Table S1) and the carbide is preserved. Details regarding preparation of the carbide supported catalysts can be found in the Supporting Information (SI).

Research described in this paper explored the use of nanostructured Mo_2C supported Pt (Pt/Mo_2C) for the water gas shift (WGS) reaction. The WGS is a critical step in the removal of CO from reformate and often accompanies steam reforming reactions during the production of hydrogen (see eq 1).[6]

$$CO + H_2O \leftrightarrow CO_2 + H_2 \quad (1)$$

Carbon monoxide is a poison for ammonia synthesis and fuel cell catalysts and has to be removed or converted prior to exposure to these catalysts.[6,7] Industrially, the WGS reaction is typically carried out in two stages: high temperature WGS (300−450 °C) using Fe-based catalysts (e.g., Fe_2O_3/Cr_2O_3) and low temperature WGS (200−270 °C) using Cu-based catalysts (e.g., $Cu/ZnO/Al_2O_3$).[6]

Recently, oxide supported Pt or Au catalysts have attracted considerable attention.[8] For these catalysts, the type of oxide has been reported to have a significant influence on the WGS rates and mechanisms.[9−15] Panagiotopoulou et al. observed that the WGS turnover frequencies (TOF), intrinsic measures of catalytic function, for Pt-based catalysts varied by as much as an order of magnitude depending on the type of oxide support.[10,11] Typically, catalysts utilizing "reducible" supports like CeO_2 and TiO_2 were more active than catalysts utilizing "irreducible" supports, such as Al_2O_3 and SiO_2. While the Pt loading and particle size affected the overall rates, the TOFs were not significantly impacted by these factors.[10] For most of these catalysts, it has been postulated that the high activities were the consequence of a bifunctional mechanism where the Pt sites adsorbed CO, and sites on the support or at the metal−support interface decomposed H_2O providing oxygen for reaction with CO.[9,13,15,16] Metals like Pt can also enhance the reducibility of the support, thus aiding in the water activation step.[12,16] A bifunctional formate decomposition mechanism has also been suggested, in particular for CeO_2 supported catalysts.[13,15,16]

Molybdenum carbide is active for the WGS with rates that can be competitive with those for commercial catalysts.[18,19] Despite its high activity, Mo_2C has not been investigated as a support for

Received: November 29, 2010
Published: February 3, 2011

dx.doi.org/10.1021/ja110705a | J. Am. Chem. Soc. 2011, 133, 2378–2381

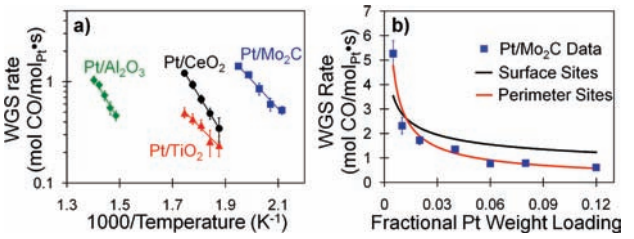

Figure 1. (a) Arrhenius plots of the WGS reaction rates for 2.7% Pt/Al_2O_3, 5% Pt/CeO_2, 2% Pt/TiO_2, and 4% Pt/Mo_2C catalysts. (b) WGS rates at 240 °C for the Pt/Mo_2C catalysts as a function of Pt loading including predicted rates from the surface site and perimeter site models described in Table S3.

Table 1. WGS Rates and Activation Energies for Supported Pt Catalysts

Catalyst	Pt Loading (wt%)	E_{App}[a] (kJ/mol)	T_{rxn}[b] (°C)	WGS Rate[c] (mol CO/ mol$_{Pt}$•s)	ref
Pt/Mo_2C	3.9	53	240	1.423	This paper
Pt/CeO_2	5.0	80	260	0.346	This paper
Pt/CeO_x	1.2	83	250	0.093[d]	20
Pt/CeO_2	0.49	--	250	0.081[e]	12
Pt/TiO_2	2.0	51	260	0.236	This paper
Pt/TiO_2	0.5	66	250	0.402[f]	11
Pt/TiO_2	0.52	--	250	0.154[e]	12

[a] Apparent activation energy. [b] Temperature for reaction rate measurement. [c] Rates for all catalysts were collected at atmospheric pressure. [d] Feed composition: 11% CO, 8% CO_2, 26% H_2, 26% H_2O, bal He. [e] Feed composition: 4.4% CO, 8.7% CO_2, 28% H_2, 29.6% H_2O, 0.1% CH_4, bal N_2. [f] Feed composition: 3% CO, 6% CO_2, 20% H_2, 10% H_2O, bal He.

WGS catalysts. In this paper we describe the preparation, evaluation, and characterization of a series of Pt/Mo_2C catalysts with Pt loadings from 0.5 to 12 wt %. The WGS rates for these materials were compared to those for a series of oxide supported Pt catalysts. Loadings for the oxide supported catalysts were controlled to achieve the same Pt surface coverage as that for the 4% Pt/Mo_2C catalyst (1.1 atom/nm^2). Results from physical and chemical characterization of these catalysts are provided in Table S2 and Figures S1 and S2.

Arrhenius plots of the WGS reaction rates are shown in Figure 1a for the 2.7% Pt/Al_2O_3, 5% Pt/CeO_2, 2% Pt/TiO_2, and 4% Pt/Mo_2C catalysts. The conversions were limited to 10% to avoid transport limitations. The reactant was designed to simulate the composition of effluent from a partial oxidation reformer and contained 11% CO, 21% H_2O, 43% H_2, 6% CO_2, and 19% N_2. The Pt/Mo_2C catalyst exhibited the highest rates while the Pt/Al_2O_3 catalyst was the least active. Rates and apparent activation energies for the oxide supported catalysts were within the range of those reported in the literature (Table 1), although the reaction conditions were slightly different from those used in our work. The Mo_2C support alone exhibited a gravimetric rate of 49 μmol/g_{cat}·s at 240 °C compared to 227 μmol/g_{cat}·s for the 4% Pt/Mo_2C catalyst. Under the same conditions, a rate of 54 μmol/g_{cat}·s was measured for a commercial Cu−Zn−Al WGS catalyst. While these results suggest that Mo_2C supported metals are promising WGS catalysts, an assessment of their methanation activity and long-term stability would be required to determine their commercial viability.

Site densities and consequently TOFs for the Pt/Mo_2C catalysts could not be experimentally estimated because CO and other typical probe molecules (e.g., H_2) were not selective chemisorbates (adsorbing, for example, on the Mo_2C support); however, insights regarding the active sites were obtained by examining the effect of Pt loading on the rates. The Pt normalized rate decreased monotonically with increasing Pt loading (see Figure 1b) suggesting that the active site density decreased with increasing Pt loading. The molar WGS rate (mol$_{CO}$/mol$_{Pt}$·s), r_{WGS}, can be described as

$$r_{WGS} = N_{sites} \bullet \mathrm{TOF} \bullet \left(\frac{\mathrm{MW_{Pt}}}{N_A \bullet W} \right) \qquad (2)$$

where N_{sites} is the active site density (sites/g_{cat}), MW_{Pt} is the atomic mass of Pt, W is the Pt loading (g_{Pt}/g_{cat}), and N_A is Avogadro's number. Assuming that the TOF and particle nucleation site density do not vary significantly with loading, relationships between r_{WGS} and W can be derived (see SI and Table S3). This latter assumption has been shown to hold for catalysts including Pt/C,[21] where the particle size increased as the Pt loading increased but no new particles were formed. The predicted WGS rates for active sites located on the particle surface or on the perimeter of the particle are shown in Figure 1b. Rates predicted by the perimeter model were more consistent with the experimental rates than those predicted by the particle surface model suggesting that active sites for the rate-determining step for WGS were at the perimeters of the Pt particles. We speculate that the CO adsorbs to Pt sites and then reacts, at the interface between Pt and the Mo_2C, with oxygen released during the reduction of H_2O on Mo_2C sites. Details regarding the WGS mechanism for these catalysts will be reported in a future publication.

In an attempt to better understand the nature of the active sites, the Pt/Mo_2C catalysts were characterized using X-ray absorption spectroscopy (XAS) and scanning transmission electron microscopy (STEM). X-ray absorption near edge structure (XANES) spectra collected at the Pt L3 edge for an unreduced 4% Pt/Mo_2C catalyst (i.e., the Mo_2C support was impregnated with $H_2PtCl_6 \cdot 6H_2O$ solution and then dried at room temperature in 1% O_2/He without further treatment) indicated that the Pt precursor was reduced by the Mo_2C surface, producing zerovalent Pt (Figure 2a). These results suggested a strong interaction between Pt and the native Mo_2C surface and the possibility of producing catalysts with high Pt dispersions. Density functional theory (DFT) calculations indicated that the binding energy of Pt to Mo_2C is 0.9 eV more favorable than the cohesive energy of Pt (see SI), which is consistent with the XANES interpretation.

Extended X-ray absorption fine structure (EXAFS) spectra were collected for a series of Pt/Mo_2C catalysts with varying Pt loadings. Figure 2b shows that the spectrum for the 4% Pt/Mo_2C catalyst was significantly different from that for a Pt foil. This spectrum is also qualitatively very similar to the spectra for the other Pt/Mo_2C catalysts with different Pt loadings (see SI). Best fits for the spectra were achieved when Mo was included in the coordination sphere around Pt (see Figure S3 and Table S4). As the Pt loading was varied, the average Pt−Pt and Pt−Mo coordination numbers (CN) remained relatively constant (Figure 2c).

dx.doi.org/10.1021/ja110705a |J. Am. Chem. Soc. 2011, 133, 2378–2381

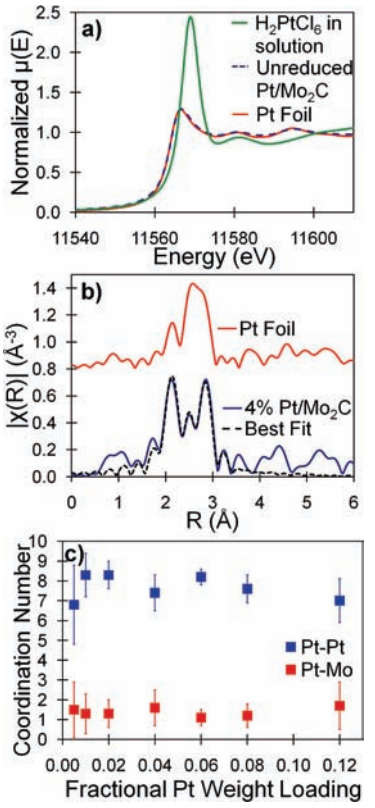

Figure 2. (a) Pt L3 XANES spectra for aqueous solution of chloroplatinic acid, unreduced 4% Pt/Mo_2C catalyst dried at room temperature in 1% O_2/He, and Pt foil. (b) EXAFS spectra for 4% Pt/Mo_2C catalyst, best-fit curve, and Pt foil. (c) Pt−Pt and Pt−Mo coordination numbers as a function of Pt loading for Pt/Mo_2C catalysts determined from EXAFS spectra.

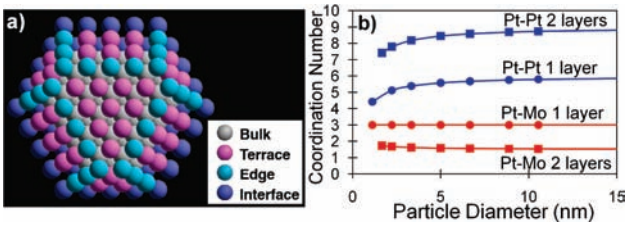

Figure 3. (a) Schematic of model Pt particle illustrating location of edge atoms, interface atoms, terrace atoms, and bulk atoms. (b) Pt−Pt and Pt−Mo coordination numbers derived from the model for a one layer thick and two layer thick Pt particle on Mo_2C.

If the particles were cuboctahedral, one would expect the average Pt−Mo CN to decrease (approaching zero as the relative number of Pt atoms bound to the Mo_2C surface decreases) and Pt−Pt CN to increase (approaching 12, the Pt−Pt coordination for bulk Pt) with increasing Pt loading. These results, combined with the XANES and DFT results, suggested the presence of raft-like Pt particles.

Geometric models were examined to better understand variations in the Pt−Pt and Pt−Mo CNs with the Pt loading (see SI). In particular, these models were used to estimate CNs for Pt particles with different diameters and thicknesses. For simplicity we assumed hexagonal particles with sides of equal length. A model particle with four layers of Pt is illustrated in Figure 3a; the edge, interface, terrace, and bulk atoms (i.e., atoms within the

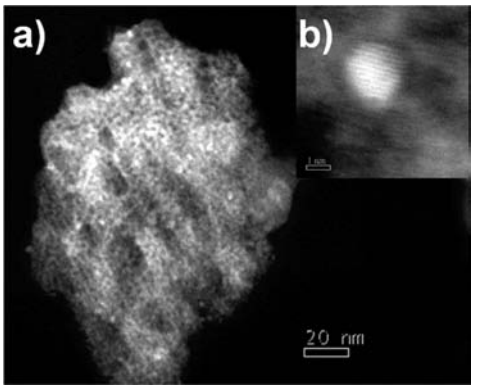

Figure 4. HAADF-STEM Electron micrographs of (a) 4% Pt/Mo_2C catalyst particle and (b) a Pt particle supported on Mo_2C.

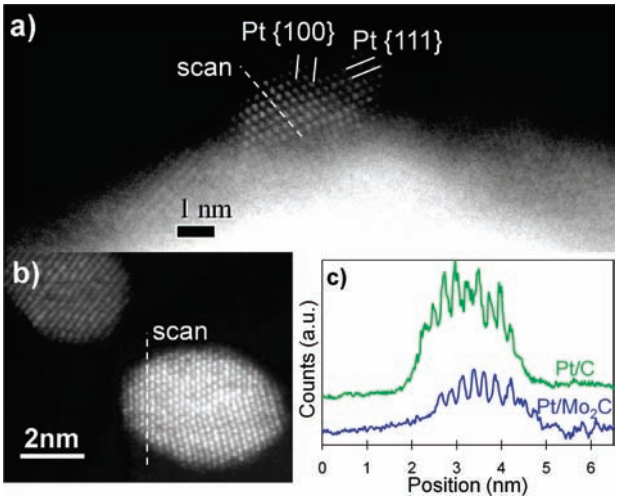

Figure 5. High resolution HAADF-STEM electron micrographs of (a) a Pt particle supported on Mo_2C and (b) a Pt particle supported on carbon. (c) Intensity line scans for the Pt particle supported on Mo_2C in Figure 5a and the Pt particle supported on carbon in Figure 5b.

particle; see Table S5) are identified. Based on DFT calculations, the Pt atoms in the first layer (interface with Mo_2C) prefer Mo hollow sites on the Mo_2C surface (Figure S4), leading to a Pt−Mo CN of 3. Average Pt−Pt and Pt−Mo CNs determined using these models were compared to those determined from the EXAFS results. Figure 3b shows the Pt−Pt and Pt−Mo CNs for one and two layer thick Pt particles as a function of particle diameter. Since the one layer thick particle is only comprised of Pt atoms on the surface of Mo_2C, the Pt−Mo CN remains constant at 3 while the Pt−Pt CN approaches 6 as the particle diameter increases. For the two layer thick Pt particle, the Pt−Mo CN approaches 1.5 and the Pt−Pt CN ranges between 7.5 and 8.8, which is in good agreement with the experimental results shown in Figure 2c. These results suggested the presence of raft-like particles where the diameter increases as the Pt loading increases, but the thickness remains approximately constant.

We used high angle annular dark field scanning transmission electron microscopy (HAADF-STEM) with C_s-correction to directly examine the particle sizes and shapes (see Figures 4 and 5). The bright spots in Figure 4a (amplified in Figure 4b) correspond to Pt particles, as confirmed by X-ray energy

dx.doi.org/10.1021/ja110705a |*J. Am. Chem. Soc.* 2011, 133, 2378–2381

dispersive spectroscopy. Most of these Pt particles were approximately 2−4 nm in size. A high resolution image of one of the particles (Figure 5a) illustrates the Pt crystallographic planes and reveals a relatively low contact angle between the Pt particle and Mo_2C support. A low contact angle is indicative of strong interactions between Pt and the Mo_2C surface. Intensity line scans (Figure 5c) for a number of particles on the Pt/Mo_2C catalyst were relatively flat compared to the rounded cuboctahedral particles on a Pt/C catalyst with similar particle sizes (Figure 5b).[22] The flatter intensity profiles were consistent over a number of Pt particles and scan directions, and the STEM results are generally consistent with the EXAFS results. Raft-like particles have higher surface area to volume (i.e., dispersions) and perimeter to volume ratios than more symmetric (e.g., cuboctahedral) particles. This particle morphology would be attractive for reactions where the rate-determining step is at the perimeter and may have contributed to the high WGS rates observed for the Pt/Mo_2C catalysts.

In summary, the Pt/Mo_2C catalysts described in this paper exhibited WGS rates that were higher than those for the oxide supported catalysts under differential conditions. High rates for the Pt/Mo_2C catalysts may have been associated with a high density of active sites at the perimeter of the Pt particles (i.e., at the interface between the Pt and the Mo_2C support). The Pt particles appeared to be raft-like due to strong interactions with the Mo_2C surface. This particle morphology is advantageous due to its high surface area to volume ratio. The strong metal−carbide interactions and the atypical particle morphologies might also occur for other carbide supported metals. Catalysts of this type could be attractive for applications where better metal utilization is required, an important challenge in particular for noble metal based fuel cell electrocatalysts.

■ ASSOCIATED CONTENT

Supporting Information. Experimental procedures, catalyst preparation and characterization, water gas shift rate measurements, density functional theory calculations, platinum particle model, active site calculations, Figures S1−S4, and Tables S1−S5 are included in the Supporting Information. This material is available free of charge via the Internet at http://pubs.acs.org.

■ AUTHOR INFORMATION

Corresponding Author
ltt@umich.edu

■ ACKNOWLEDGMENT

The authors acknowledge financial support from the National Science Foundation (CBET 0933239) and Michigan Memorial Phoenix Energy Institute. The HAADF-STEM was performed in the Electron Microbeam Analysis Laboratory at the University of Michigan (JEOL 2100F STEM, NSF Grant DMR 0723032), and the XAS was performed at the Advanced Photon Source at Argonne National Laboratory with the assistance of members of the Materials Research Collaborative Access Team (supported by the Department of Energy and the MRCAT member institutions).

■ REFERENCES

(1) Lee, J. S.; Locatelli, S.; Oyama, S. T.; Boudart, M. *J. Catal.* **1990**, *125*, 157–170.
(2) Ledoux, M. J.; Pham-Huu, C.; Chianelli, R. R. *Curr. Opin. Solid State Mater. Sci.* **1996**, *1*, 96–100.
(3) Oyama, S. T. *Catal. Today* **1992**, *15*, 179–200.
(4) Lewandowski, M.; Szymanska-Kolasa, A.; Da Costa, P.; Sayag, C. *Catal. Today* **2007**, *119*, 31–34.
(5) Griboval-Constant, A.; Giraudon, J.-M.; Leclercq, G.; Leclercq, L. *Appl. Catal. A: General* **2004**, *260*, 35–45.
(6) Bartholomew, C. H.; Farrauto, R. J. *Fundamentals of Industrial Catalytic Processes*, 2nd ed.; John Wiley and Sons: 2006.
(7) Ladebeck, J. R.; Wagner, J. P. In *Handbook of Fuel Cells − Fundamentals, Technology, and Applications*; Vielstich, W., Lamm, A., Gasteiger, H. A., Eds.; Wiley: 2003.
(8) Fu, Q.; Saltsburg, H.; Flytzani-Stephanopoulos, M. *Science* **2003**, *301*, 935–938.
(9) Boisen, A.; Janssens, T. V. W.; Schumacher, N.; Chorkendorff, I.; Dahl, S. *J. Mol. Catal. A: Chemical* **2010**, *315*, 163–170.
(10) Panagiotopoulou, P.; Kondarides, D. *Catal. Today* **2006**, *112*, 49–52.
(11) Panagiotopoulou, P.; Kondarides, D. *Catal. Today* **2007**, *127*, 319–329.
(12) Gonzalez, I. D.; Navarro, R. M.; Wen, W.; Marinkovic, N.; Rodriguez, J. A.; Rosa, F.; Fierro, J. L. G. *Catal. Today* **2010**, *149*, 372–379.
(13) Iida, H.; Igarashi, A. *Appl. Catal. A: General* **2006**, *298*, 152–160.
(14) Phatak, A. A.; Koryabkina, N.; Rai, S.; Ratts, J. L.; Ruettinger, W.; Farrauto, R. J.; Blau, G. E.; Delgass, W. N.; Ribeiro, F. H. *Catal. Today* **2007**, *123*, 224–234.
(15) Azzam, K. G.; Babich, I. V.; Seshan, K.; Lefferts, L. *J. Catal.* **2007**, *251*, 163–171.
(16) Jacobs, G.; Graham, U. M.; Chenu, E.; Patterson, P. M.; Dozier, A.; Davis, B. H. *J. Catal.* **2005**, *229*, 499–512.
(17) Kalamaras, C. M.; Panagiotopoulou, P.; Kondarides, D. I.; Efstathiou, A. M. *J. Catal.* **2009**, *264*, 117–129.
(18) Moon, D. J.; Ryu, J. W. *Catal. Lett.* **2004**, *92*, 17–24.
(19) Patt, J.; Moon, D. J.; Phillips, C.; Thompson, L. *Catal. Lett.* **2000**, *65*, 193–195.
(20) Pierre, D.; Deng, W.; Flytzani-Stephanopoulos, M. *Top. Catal.* **2007**, *46*, 363–373.
(21) Voropaev, I. N.; Simonov, P. A.; Romanenko, A. V. *Russ. J. Inorg. Chem.* **2009**, *54*, 1531–1536.
(22) Ferreira, P. J.; la O', G. J.; Shao-Horn, Y.; Morgan, D.; Makharia, R.; Kocha, S.; Gasteiger, H. A. *J. Electrochem. Soc.* **2005**, *152*, A2256–A2271.